APL MATERIALS **2**, 012109 (2014)

Size-dependent mobility of gold nano-clusters during growth on chemically modified graphene

Gavin R. Bell,[1,a] Peter M. Dawson,[1] Priyanka A. Pandey,[1] Neil R. Wilson,[1] and Paul A. Mulheran[2]
[1]*Department of Physics, University of Warwick, Coventry CV4 7AL, United Kingdom*
[2]*Department of Chemical and Process Engineering, University of Strathclyde, James Weir Building, 75 Montrose St., Glasgow G1 1XJ, United Kingdom*

(Received 21 November 2013; accepted 8 January 2014; published online 24 January 2014)

Gold nano-clusters were grown on chemically modified graphene by direct sputter deposition. Transmission electron microscopy of the nano-clusters on these electron-transparent substrates reveals an unusual bimodal island size distribution (ISD). A kinetic Monte Carlo model of growth incorporating a size-dependent cluster mobility rule uniquely reproduces the bimodal ISD, providing strong evidence for the mobility of large clusters during surface growth. The cluster mobility exponent of −5/3 is consistent with cluster motion via one-dimensional diffusion of gold atoms around the edges of the nano-clusters. [http://dx.doi.org/10.1063/1.4862696]

The study of material nucleating and growing on a solid surface has a history of many decades, ranging from the thermodynamics of liquid droplets on solids to contemporary molecular dynamics simulations at the bio-materials interface.[1–7] Deposition and growth systems are typically characterised by huge ranges of time and length scale: the microscopic processes of surface growth (atomic length scale, time scale $\sim 10^{-12}$ s) aggregate to produce thin films, clusters or patterns with length scales from nm to μm over time scales of seconds or minutes.[8,9] While the microscopic processes are not usually directly accessible to experiment, their nature can often be inferred from the statistical properties of the grown material, for example, the island size distribution (ISD)[1] or the spatial distribution of islands[10] and their associated capture zones.[11] A particularly powerful tool in this regard is kinetic Monte Carlo (KMC) simulation, which can efficiently bridge the time and length scale gaps. The simplest flavour of KMC model requires that all the possible elementary processes and their rates be defined *a priori*. These may be defined through detailed microscopic calculations, e.g., via density functional theory (DFT),[12] or with the aid of a comparison of the statistical properties of simulated and measured growth structures.[13] In this work, we adopt the latter approach. We show that large clusters (containing hundreds or thousands of atoms) are able to move on the time scale of the growth and that this motion profoundly influences the ISD, producing a characteristic bimodal distribution.

Experimental analysis of sub-μm growth structures is usually achieved by scanning probe microscopy (SPM). While SPM can provide high spatial resolution and true 3D topography, there are some disadvantages. First, SPM image acquisition is normally quite slow and it can be challenging to build large data sets for extraction of a statistically robust ISD. Second, if the topographic steepness of the grown structures is comparable to the sharpness of the probe tip, convolution with the tip shape distorts the measured island sizes.[14] An attractive complementary method is transmission electron microscopy (TEM) which can combine high spatial resolution with rapid acquisition of images. However, the growth structures must sit on an electron-transparent substrate in order to

[a]Author to whom correspondence should be addressed. Electronic mail: gavin.bell@warwick.ac.uk

image by TEM. Two-dimensional (2D) materials such as graphene or chemically modified graphene (CMG) can be used as strong and highly electron-transparent substrates.[15,16] In the particular case of graphene and CMG, it is also important to understand the substrate interaction with films and nano-clusters, since these hybrid systems may underpin new graphene-based technologies.[17] Such arrays of metallic nano-clusters have potential application in fields such as catalysis, plasmonics, and sensing,[18–20] for which it is important to control nanoparticle ISD and spacing. As a recent example of a hybrid material system, a study of graphene/Al_2O_3/Au nano-clusters found that the Au surface plasmon resonance could be tuned via the Al_2O_3 spacer thickness due to interaction with image charges in the graphene.[21] A sound understanding of both elementary growth processes and cluster interactions on the substrate will underpin efforts to control scalable self-assembly processes for hybrid graphene nano-materials.

Here, we describe the formation of Au nano-clusters on CMG. These are self-assembled purely by growth in conventional sputter deposition (deposition of Au monomers). The ISDs are measured by TEM with high statistical fidelity and have an unusual bimodal nature. This cannot be reproduced by KMC modelling with conventional processes (irreversible aggregation of immobile clusters) and so we introduce a size-dependent cluster mobility. This allows the ISDs to be reproduced accurately and strongly suggests that the mechanism for cluster mobility is one-dimensional (1D) diffusion of Au atoms around the perimeter of Au clusters.

The CMG was prepared by a modified Hummers method, resulting in mainly single-sheet graphene oxide which was mounted on standard lacy carbon TEM grid supports.[15] Gold was deposited directly onto these CMG-on-TEM-grid substrates at room temperature in a standard metal sputtering system. The deposition rate was fixed (0.07 nm s^{-1}) and several coverages up to nominally 1.5 nm were deposited. Under these conditions, Au forms nano-clusters rather than continuous films.[16] The coverages θ are defined by comparison to Au-on-metal thin film growth: while absolute values are nominal, the relative quantity of deposited Au between different coverages is accurate. The growth is not epitaxial, with electron diffraction clearly showing the lattice planes of Au nano-clusters oriented randomly with respect to the CMG. In larger clusters of several nm diameter, usually several sets of lattice planes of Au could be imaged in high resolution TEM (HRTEM), indicating a three-dimensional (3D) compact cluster shape.[16] For the smallest islands, <1 nm diameter, though still compact in plan-view, no such lattice images were observed and the overall contrast was weaker. This indicates thinner structures and, while detailed image interpretation of such small islands is difficult due to the mixing of diffraction and atomic number contrast in HRTEM, the observations are consistent with a 2D morphology for such clusters.

Having deposited the Au, the grids were transferred through air and imaged using conventional TEM (Jeol 2000FX and 2100 LaB_6 microscopes operating at 200 kV). For each coverage, a series of images ($\sim 450 \times 300$ nm^2, magnification 60 000×) was obtained, from which the ISDs were extracted after thresholding using the Fiji image processing package.[22] The Au clusters were stable under these imaging conditions. However, during HRTEM imaging, where the incident electron flux is much higher, clusters were sometimes seen to move during imaging. This observation initially motivated our KMC investigation of cluster mobility during the growth. The ISDs are each based on several representative images totalling at least 10^4 islands at each coverage. They are displayed as continuous probability densities (Gaussian kernel estimation method) rather than as histograms (binning method). The KMC-derived ISDs are binned and in all cases the bimodality of the ISDs is clear and easily comparable. The ISDs are represented as the probability density distributions of island diameter scaled to the Au(111) lattice parameter (0.288 nm). This is a simple and reliable measure of island size since in the low coverage regime ($\theta < 1$ nm) only a small fraction of the observed islands have a non-compact shape. At 1.5 nm coverage, many islands are non-compact due to coalescence of larger clusters,[16] and we do not analyse this regime here.

We now describe the KMC model and its parameterization. The model is based on a simulation grid on which islands (Au nano-clusters) and monomers (Au atoms) can diffuse and interact. The model is constructed on a square grid scaled to the lattice spacing of Au. The Au islands are assumed to be either circular or hemispherical and hence have nonzero area. Random deposition of Au atoms occurs at a fixed rate. Diffusion of Au adatoms on the grid occurs through nearest neighbour hopping such that the diffusion constant is R times that of the monolayer deposition rate. As usual in such

growth simulations, the parameter R strongly influences the evolution of the system: high R produces fewer, larger islands while low R favours independent nucleation to give more numerous, smaller islands. Adatoms which meet islands during surface diffusion aggregate irreversibly, but the islands themselves are allowed to move according to a rule described below. When two islands touch they are assumed to instantly form a new hemispherical island with the combined number of monomers, a reasonable approximation given the compact cluster shapes which dominate the experimental images in the low coverage regime of interest. To reflect TEM observations,[16] we assume that islands smaller than a critical size s_{crit} are circular (2D), and these transition to a hemispherical island shape (3D) at larger sizes.

The length scale and connectivity of the simulation grid are not critical provided that the grid is sufficiently fine to properly capture the statistical properties of the real diffusion pathways. At a given grid scale, the area covered by an island is determined by the number of atoms in the island and the island shape. For a sufficiently fine grid, changes of grid scale at fixed real island separation can be compensated for by changing the rate of hopping through R, keeping the diffusion constant the same for all grid scales. The simulations were checked by altering the grid scale to match Au(111), Au(001), or graphene lattice spacing. We confirmed that these changes of grid scale did *not* affect the simulations.

The cluster mobility rule gives the probability $p(s)$ for a cluster of size s atoms to diffuse. In typical growth simulations, clusters of size $s > 1$ do not move and only monomers are mobile, though some recent simulation work has addressed cluster mobility.[23–25] In the present work, we examined different cluster mobility rules and found the following form (Eq. (1)) allowed good reproduction of the experimental size distributions,

$$p(s) = \begin{cases} 1 \text{ if } s = 1 \\ 0 \text{ if } 1 < s < s_{crit} \\ 1/s^{\alpha} \text{ if } s \geq s_{crit}. \end{cases} \quad (1)$$

Monomers (isolated adatoms) always diffuse, whereas clusters containing more than 1 atom are immobile and 2D, until they grow to a size s_{crit}. Then diffusion can take place with a probability decreasing with exponent α as the size increases, and these mobile islands are modelled as 3D hemispheres as discussed above. Hence, the three free parameters of the simulation are: the diffusion/deposition ratio R, the critical cluster size s_{crit}, and the cluster mobility exponent α. Since experiments were performed at fixed deposition rate and substrate temperature, R was identical for all Au coverages for the same choice of lattice scale. Here, we set the lattice scale to the Au(111) lattice parameter and proceed to determine the simulation parameters by comparison with experiment, as discussed below.

Representative 180 nm sections of experimental images at two coverages (0.15 nm and 0.75 nm) are shown in Fig. 1. The Au nano-clusters appear as dark spots on the slightly mottled light grey background due to the CMG support. The lower right part of image (a) is expanded to show some individual islands more clearly: even very small (<1 nm) islands are readily distinguishable due to the high transparency of the CMG substrate. In the lower right section of panel (b) is shown the effect of thresholding to produce the binary images used to generate ISDs. The image processing steps were varied to check their effect on the ISD, which were negligible. Panels (c) and (d) of Fig. 1 show the equivalent KMC simulations produced with optimized parameters. There is an excellent "by-eye" correspondence between the KMC and TEM images, with the average island size increasing at high coverage even though a large number of very small islands remain. In the experimental images, island coalescence appears to be just starting by $\theta \approx 0.75$ nm and, even though non-compact shapes are not allowed in the KMC model, it is clear that some islands are nearly touching and/or filling their capture zones at this coverage (panel (d), bottom right). This indicates that the island size and number density behaviours are approximately correct in the model.

The experimental ISDs at coverages of 0.15 nm and 0.75 nm are shown in Fig. 2. The distributions are clearly bimodal with a significant number of very small islands alongside a broad distribution of larger islands. The very small islands show weaker contrast and no lattice fringes in HRTEM, consistent with a 2D morphology. The larger islands' average size increases as the growth proceeds,

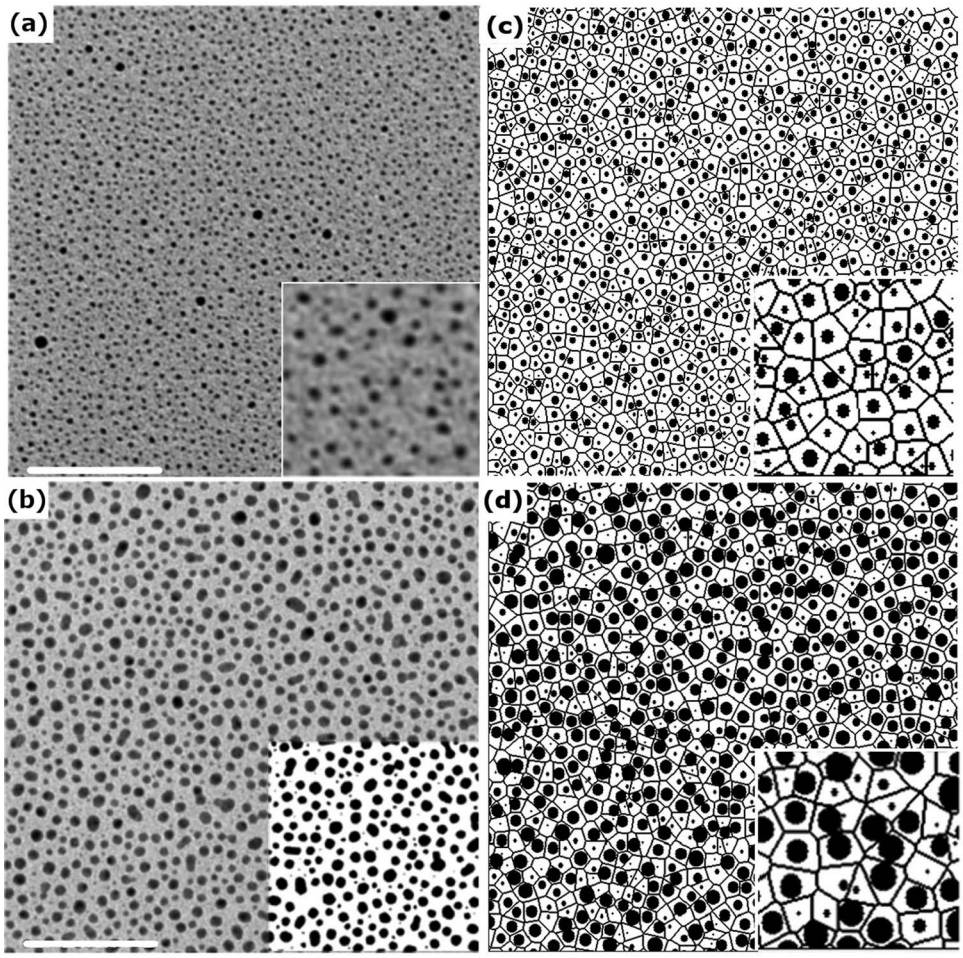

FIG. 1. Representative sections (180 × 180 nm^2, white scale bar 50 nm) from larger TEM images of Au nano-clusters on CMG, at nominal Au coverages of (a) 0.15 nm and (b) 0.75 nm. The bottom right section of panel (a) shows a further 2× zoom of the image while in panel (b) the bottom right image section has been thresholded to produce the binary image used in particle analysis. In panels (c) and (d) are shown KMC simulation outputs on a grid of approximately equivalent size, where the black circles represent Au nano-clusters and the Voronoi cell about each cluster (its capture zone) is also shown. The bottom right sections of these panels again show 2× zooms for clarity.

while the distribution of smallest islands remains centred about approximately the same diameter. The corresponding ISDs from simulation are also given in Fig. 2. In the model, the low-size peaks of the ISDs comprise only immobile 2D islands. The key features of the ISD evolution are reproduced by the KMC model: the distributions are bimodal and the small-island component does not evolve in size during growth, while the large-island component does increase in size with decreasing peak probability density. While the simulated ISDs do not precisely match the experimental peak positions and weights, the agreement is strikingly good.

It was impossible to simulate even the qualitative form of the experimental ISDs without including cluster mobility. Furthermore, a rule of the kind given in Eq. (1) was essential—for example, setting $s_{\text{crit}} = 0$ or not suppressing the mobility of largest islands always failed to produce ISDs resembling the bimodal experimental data, even when other parameters were varied. Having decided on the cluster mobility rule, optimised simulations were produced by varying only the three parameters R, s_{crit} and α. Figures 3 and 4 give an indication of how this tractable parameter space affects the simulated ISDs, concentrating on $\theta \approx 0.75$ nm. In Fig. 3, the diffusion/deposition ratio R is varied by an order of magnitude either side of the optimum value (6×10^4, open diamonds). This has a strong effect on the peak of larger islands: as R increases, these islands become bigger with a

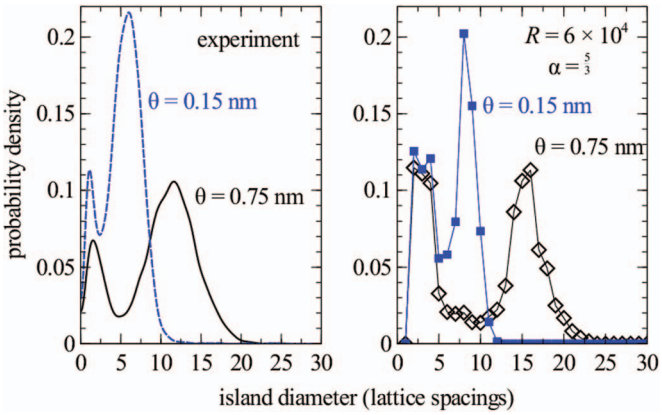

FIG. 2. Experimental (left) and optimised simulation (right) ISDs for Au nano-clusters on CMG at nominal Au coverages of 0.15 nm and 0.75 nm.

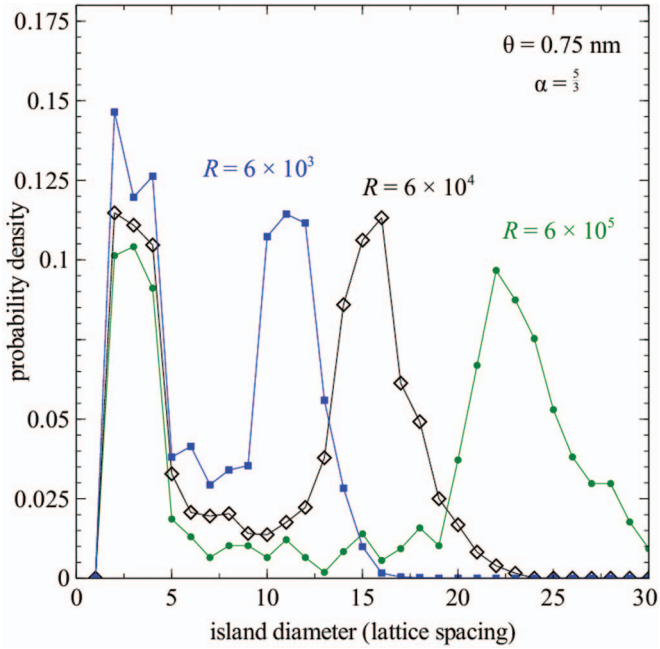

FIG. 3. Simulation ISDs for Au nano-clusters on CMG at nominal Au coverage of 0.75 nm, varying the diffusion/deposition ratio *R*. The optimum parameter set is shown as open diamonds to match Fig. 1.

slightly broader distribution, as expected. Note that the total density of islands varies strongly with *R*, providing another means to determine its optimal value by comparison with the experimental data (see Fig. 1). Furthermore, the small-island peaks are hardly affected by varying *R* (Fig. 3). The insensitivity of the lower peak to *R* is very useful when finding s_{crit}, which is strongly constrained by the position of the small-island peak in the ISDs. When islands grow larger than s_{crit}, they are able to find other islands into which they merge, producing a dip in the ISD. Therefore, s_{crit} can be set reasonably independently of other parameters at a monomer number close to that corresponding to diameter of the lower ISD peak. The optimum value of s_{crit} was 10 atoms.

This leaves the cluster mobility exponent α. One would expect different values of α depending on the dominant physical process giving rise to cluster mobility.[26,27] Six candidate mechanisms are considered:

i. Surface evaporation and condensation of Au atoms at the upper free surfaces of the clusters;
ii. Evaporation and condensation onto the CMG substrate at the cluster edges;

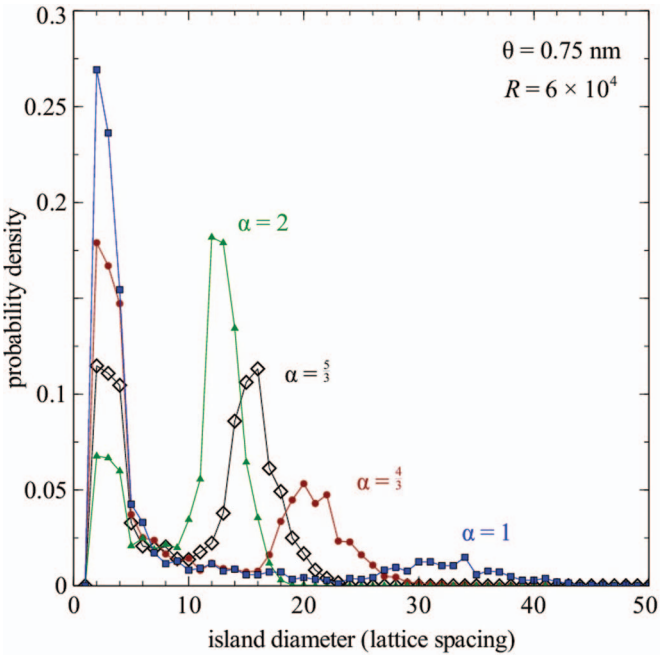

FIG. 4. Simulation ISDs for Au nano-clusters on CMG at nominal Au coverage of 0.75 nm, varying the cluster mobility exponent α.

TABLE I. Elementary diffusion mechanisms supporting cluster mobility and their dependence on attempt frequency ν, centre of mass (CoM) hop length a and cluster size s. Only α, the exponent of s in the diffusion constant, varies between mechanisms, and only $\alpha = 5/3$ is consistent with measured ISDs, implying 1D edge diffusion as the origin of cluster mobility.

	Mechanism	Number density (frequency)	CoM hop length	Diffusion constant
i	Atop evaporation/condensation	$\nu s^{2/3}$	$as^{-2/3}$	$\nu a^2 s^{-2/3}$
ii	Edge evaporation/condensation	$\nu s^{1/3}$	$as^{-2/3}$	$\nu a^2 s^{-1}$
iii	2D interface diffusion	$\nu s^{2/3}$	as^{-1}	$\nu a^2 s^{-4/3}$
iv	2D atop diffusion	$\nu s^{2/3}$	as^{-1}	$\nu a^2 s^{-4/3}$
v	1D edge diffusion	$\nu s^{1/3}$	as^{-1}	$\nu a^2 s^{-5/3}$
vi	Point-like contact	ν	as^{-1}	$\nu a^2 s^{-2}$

iii. 2D diffusion of Au atoms at the interface between the cluster and CMG;
iv. 2D diffusion of Au atoms across the top of the gold cluster;
v. 1D diffusion of Au atoms around the edge of the Au cluster at the CMG interface;
vi. Point-like contact between cluster and substrate with diffusion of contacting atom.

In each case, the number density of migrating monomer species, the hopping length, and hence the associated diffusion coefficient of the cluster will scale differently with cluster size s. Following Wen *et al.*,[26] this scaling is summarised in Table I and examples of the effects of α are shown in Fig. 4. Only the exponent α varies between mechanisms, allowing the mechanism to be inferred (at least from the list considered) if α can be determined by comparison of the ISDs. This is indeed the case, with smaller values of α shifting the large-island peak to higher diameters while at the same time broadening it and reducing its weight in comparison to the small-island peak (Fig. 4). The strength of this effect and its contrast with the effect of R is sufficient to allow α to be identified as 5/3 from among the candidate values. This strongly suggests that 1D diffusion of Au monomers around the edges of the Au clusters is responsible for their mobility.

The three free parameters of the model have been determined quasi-independently. The exact numerical value of R is not so important given that different experimental growth conditions (substrate

temperature, growth rate) would be expected to change it; values much greater than unity are expected for such nano-cluster growth.[1] The value of α implies that 1D edge diffusion of Au is likely to cause island mobility. This is consistent with the small size of s_{crit} below which edge diffusion would involve Au atoms in unfavourable low-coordination sites, and is likely related to a change of nano-cluster morphology from flatter islands to a more 3D compact shape which enables 1D edge diffusion. While both the abrupt onset of island mobility at s_{crit} (Eq. (1)) and the abrupt shape change from circular to hemispherical are clearly simplifications, the general form of the size-dependent cluster mobility required to reproduce the experimental ISDs is robust. Further microscopic study of the smallest clusters, both experimentally and via a fine-grained simulation approach such as DFT, should shed more light on the atomistic behaviour associated with cluster mobility and morphology.

See the supplementary material[28] for a short movie showing a run of the KMC model at its optimum parameters, ending with a final fractional coverage corresponding to $\theta = 0.75$ nm (Figs. 1(b) and 1(d)). Several features of the growth are evident from observing this movie. The largest islands are essentially immobile but smaller islands are able to migrate across a capture zone to join a large island or merge with each other. Second, nucleation continues throughout, serving to "top up" the number density of smallest islands. Such nucleation often occurs in larger Voronoi cells recently expanded by an island merging event. Although the simulation does not allow non-compact island shapes, the rate at which medium-sized or large islands merge later in the simulation, which would give rise to the non-compact shapes beginning to appear at $\theta = 0.75$ nm, appears qualitatively correct as the growth proceeds. The rate of change of capture zone structure reduces throughout the growth as more islands become immobile, but the Voronoi cell pattern does not completely stabilise due to the continued nucleation.

In summary, we have combined TEM and KMC simulation in a study of Au nano-cluster growth on CMG. We have measured unusual bimodal ISDs which can be explained by allowing Au nano-clusters of sufficient size to be mobile on the CMG surface, consistent with a possible 2D-to-3D transition in island morphology. Fitting of the statistically robust experimental ISDs to such a model suggests strongly that the mechanism for island mobility is 1D diffusion of Au atoms around the island base perimeter.

We are grateful to B. J. Hickey and M. D. Elkin for the Au sputter deposition, to J. P. Rourke for CMG preparation, and to S. York for technical support. The Gatan Orius digital TEM camera used in this research was funded by Birmingham Science City: Creating and Characterising Next Generation Advanced Materials, with support from Advantage West Midlands and partly funded by the European Regional Development Fund. The Warwick Centre for Complexity Science provided studentship support for P. Dawson through its EPSRC Doctoral Training Centre.

[1] M. Einax, W. Dieterich, and P. Maass, Rev. Mod. Phys. **85**, 921 (2013).
[2] R. P. Sear, Int. Mater. Rev. **57**, 328 (2012).
[3] H. Brune, Surf. Sci. Rep. **31**, 125 (1998).
[4] J. W. Evans, P. A. Thiel, and M. C. Bartelt, Surf. Sci. Rep. **61**, 1 (2006).
[5] P. A. Mulheran, D. Pellenc, R. A. Bennett, R. J. Green, and M. Sperrin, Phys. Rev. Lett. **100**, 068102 (2008).
[6] K. Kubiak-Ossowska and P. A. Mulheran, Langmuir **28**, 15577 (2012).
[7] D. Quigley, P. M. Rodger, C. L. Freeman, J. H. Harding, and D. M. Duffy, J. Chem. Phys. **131**, 094703 (2009).
[8] D. D. Vvedensky, J. Phys.: Condens. Matter **16**, R1537 (2004).
[9] M. Basham, F. Montalenti, and P. A. Mulheran, Phys. Rev. B **73**, 045422 (2006).
[10] T. Konishi and S. Tsukamoto, Surf. Sci. **605**, L1 (2011).
[11] P. A. Mulheran, Europhys. Lett. **65**, 379 (2004).
[12] P. Kratzer and M. Scheffler, Phys. Rev. Lett. **88**, 036102 (2002).
[13] M. Itoh, G. R. Bell, A. R. Avery, T. S. Jones, B. A. Joyce, and D. D. Vvedensky, Phys. Rev. Lett. **81**, 633 (1998).
[14] T. J. Krzyzewski, P. B. Joyce, G. R. Bell, and T. S. Jones, Phys. Rev. B **66**, 201302(R) (2002).
[15] N. R. Wilson *et al.*, ACS Nano **3**, 2547 (2009).
[16] P. Pandey, G. R. Bell, J. P. Rourke, A. M. Sanchez, M. D. Elkin, B. J. Hickey, and N. R. Wilson, Small **7**, 3202 (2011).
[17] K. S. Novoselov, V. I. Fal'ko, L. Colombo, P. R. Gellert, M. G. Schwab, and K. Kim, Nature (London) **490**, 192 (2012).
[18] M. Pelton, J. Aizpurua, and G. Bryant, Laser Photonics Rev. **2**, 136 (2008).
[19] M.-A. Neouze, J. Mater. Sci. **48**, 7321 (2013).
[20] P. A. Pandey, N. R. Wilson, and J. A. Covington, Sens. Actuators **183**, 478 (2013).
[21] J. Niu, Y. J. Shin, Y. Lee, J.-H. Ahn, and H. Yang, Appl. Phys. Lett. **100**, 061116 (2012).
[22] J. Schindelin *et al.*, Nat. Methods **9**, 676 (2012).
[23] Y. A. Kryukov and J. G. Amar, Phys. Rev. E **83**, 041611 (2011).

[24] P. A. Mulheran and M. Basham, Phys. Rev. B **77**, 075427 (2008).
[25] P. A. Mulheran and D. A. Robbie, Phys. Rev. B **64**, 115402 (2001).
[26] J.-M. Wen, S.-L. Chang, J. W. Burnett, J. W. Evans, and P. A. Thiel, Phys. Rev. Lett. **73**, 2591 (1994).
[27] C. DeW. Van Siclen, Phys. Rev. Lett. **75**, 1574 (1995).
[28] See supplementary material at http://dx.doi.org/10.1063/1.4862696 for an AVI-format movie of the KMC model at optimized parameters.